ISSN 1063-7729, Astronomy Reports, 2018, Vol. 62, No. 1, pp. 9–18. © Pleiades Publishing, Ltd., 2018.
Original Russian Text © T.G. Elizarova, A.A. Zlotnik, M.A. Istomina, 2018, published in Astronomicheskii Zhurnal, 2018, Vol. 95, No. 1, pp. 11–21.

Hydrodynamical Aspects of the Formation of Spiral–Vortical Structures in Rotating Gaseous Disks

T. G. Elizarova[1*], A. A. Zlotnik[2], and M. A. Istomina[1]**

[1] *Keldysh Institute of Applied Mathematics, Moscow, 125047 Russia*

[2] *National Research University Higher School of Economics, Moscow, 101000 Russia*

Received May 24, 2017; in final form, September 5, 2017

Abstract—This paper is dedicated to numerical simulations of spiral–vortical structures in rotating gaseous disks using a simple model based on two-dimensional, non-stationary, barotropic Euler equations with a body force. The results suggest the possibility of a purely hydrodynamical basis for the formation and evolution of such structures. New, axially symmetric, stationary solutions of these equations are derived that modify known approximate solutions. These solutions with added small perturbations are used as initial data in the non-stationary problem, whose solution demonstrates the formation of density arms with bifurcation. The associated redistribution of angular momentum is analyzed. The correctness of laboratory experiments using shallow water to describe the formation of large-scale vortical structures in thin gaseous disks is confirmed. The computations are based on a special quasi-gas-dynamical regularization of the Euler equations in polar coordinates.

DOI: 10.1134/S1063772918010018

1. INTRODUCTION

Investigation of evolutionary processes occurring in various types of accretion disks is a currently actively studied area of astrophysics (see, e.g., [1–8]). According to [4, 5], the spiral structure of "nebulae" was first noted in observations obtained by Lord Rosse in 1845. Later, spiral arms and gigantic vortices—cyclones and anticyclones—were discovered in the two-dimensional velocity fields of the gaseous disks of a number of galaxies. The spirals are categorized according to their shapes. Lagging spirals are most often encountered, which rotate with their ends backward and have a naturally aerodynaical form. Branching of the spirals is a widespread phenomenon, in which the arms are bifurcated in the direction of their ends. Galactic disks in the form of concentric rings are also observed.

Mechanisms for the appearance of spiral–vortical structures in astrophysical objects—galaxies and accretion disks—were discussed in [2, 4, 5]. In particular, the generation of spiral density waves was related to the non-linear interaction of gravitational and hydrodynamical instability, which in real galaxies could arise due to a rapid local drop in the rotational velocity of the gas. This is clearly visible in the observed rotation curves of galaxies.

Rotating shallow water was used to experimentally model the generation of spiral structure in a gaseous galactic disk caused by the development of hydrodynamical instability due to the presence of a gradient in the rotational velocity. In particular, the correctness of the gravitational–hydrodynamical theory of the generation of this spiral structure was confirmed on the "Spiral" installation. Bifurcation of the spiral arms was observed, as well as anticyclonic vortices [2].

Theoretical studies of the stability of astrophysical gaseous and galactic disks have been carried out since the 1940s. The results obtained and an extensive bibliography are presented in [4, 7, 9]. Various aspects of the development of small perturbations have mainly been studied in the framework of linear theories and spectral expansions.

An accretion disk is a rotating gaseous formation in the vicinity of a compact gravitating center. This situation can be described using the Euler equations of gas dynamics, implementing a spatial resolution for which the cell size appreciably exceeds the characteristic mean free path of a molecule in the gaseous disk.

Numerical simulations of gravitational instabilities in accretion disks have been carried out, for example, in [10–13]. Since the role of viscosity is expected to be negligle in the generation of spiral arms in real galaxies [4], these computations were based on solving the Euler equations (without viscous terms). Mathematical modeling of gas-dynamical flows in an

*E-mail: telizar@mail.ru
**E-mail: azlotnik@hse.ru

accretion disk using new computational approaches can potentially both confirm the behavior observed earlier and reveal new properties of the evolution of such flows.

As a means of supplementing earlier studies, it is of considerable interest to apply the apparatus of direct numerical simulations to verify the hypothesis that the arms in gaseous disks have a purely hydrodynamical nature, and to test the analogy between gravitational instability in gaseous disks and in flows in shallow water. The aim of our current study is to analyze these questions applying a simple model based on the two-dimensional, non-stationary, barotropic Euler equations with a body force in polar coordinates. This formulation of the problem does not aspire to a full description of the physics of accretion disks, but is overall consistent with a fairly standard approach [12].

The inputs to the computations were the initial distributions of the density and velocity, which were derived for a stationary, three-dimensional configuration in a barotropic approximation in [10]. In contrast to [1–12], we reduce the three-dimensional problem to a two-dimensional one by applying not an approximate but an *exact* averaging of the original equations in the vertical coordinate. A deciding role is played by averaging the enthalpy rather than the density. Moreover, the stationary solutions are constructed not only for an isentropic flow (for adiabatic index $\gamma > 1$), but also for an isothermal flow, often discussed in the literature ($\gamma = 1$).

These new axially symmetric, stationary solutions were used to provide the initial distribution (with small perturbations) for the non-stationary equations. We do not consider the stability of the initial distributions against small perturbations analytically in this study, but it is known on physical grounds that a barotropic gas flow in a gravitational field is unstable [3, 4].

In contrast to [10–12], we solved this problem using the Euler equations in a barotropic application, which is fairly natural when constructing the initial distributions precisely in this framework. The numerical algorithm applied is based on a difference approximation of the initially regularized (quasi-gas-dynamical, QGD) equations, adapted for this problem. The equations and their difference analogs are written in polar coordinates. QGD algorithms have been used earlier in computations of a wide range of gaseous and hydrodynamical flows [14–16], including modeling shallow water flows [17].

The paper is organized as follows. Section 2 presents the gas-dynamical equations in the barotropic approximation in polar coordinates. The new stationary solutions are constructed. Section 3 presents the regularized (QGD) equations, and describes the numerical algorithm in general terms. The results of the numerical simulations are presented in Section 4, and the main results are summarized in Section 5. Note that additional details and the first results of this study were presented in [18].

2. BAROTROPIC GAS-DYNAMICAL EQUATIONS IN POLAR COORDINATES AND THEIR STATIONARY SOLUTIONS

The system of barotropic Euler equations in polar coordinates (r, φ) includes the following mass and momentum balance equations:

$$\frac{\partial \rho}{\partial t} + \nabla \cdot (\rho \mathbf{u}) = 0, \tag{1}$$

$$\frac{\partial (\rho u_r)}{\partial t} + \nabla \cdot (\rho u_r \mathbf{u}) + \frac{\partial p(\rho)}{\partial r} - \frac{\rho u_\varphi^2}{r} = \rho f_r, \tag{2}$$

$$\frac{\partial (\rho u_\varphi)}{\partial t} + \frac{1}{r}\nabla \cdot (r \rho u_\varphi \mathbf{u}) + \frac{1}{r}\frac{\partial p(\rho)}{\partial \varphi} = \rho f_\varphi, \tag{3}$$

where $\rho(r, \varphi, t)$ is the density, $\mathbf{u} = (u_r, u_\varphi)$ the velocity vector, $u_r(r, \varphi, t)$ and $u_\varphi(r, \varphi, t)$ the radial and azimuthal velocity components, and $\nabla \cdot \mathbf{v} = \frac{1}{r}\frac{\partial (r v_r)}{\partial r} + \frac{1}{r}\frac{\partial v_\varphi}{\partial \varphi}$ is the divergence of the vector function $\mathbf{v} = (v_r, v_\varphi)$. Further, $p(\rho) = p_0(\rho/\rho_0)^\gamma = k\rho^\gamma$ is the gas pressure, where $\gamma = \text{const} \geq 1$ is the adiabatic index and the coefficient $k = p_0/\rho_0^\gamma > 0$ determines the constant specific entropy of the flow when $\gamma > 1$ (the isentropic case) or the constant temperature when $\gamma = 1$ (the isothermal case). The sound speed is $c_s = \sqrt{\gamma p(\rho)/\rho}$. The quantities f_r and f_φ are the radial and azimuthal components of the external body force.

Stationary gas-dynamical equations with a gravitational force were studied in a cylindrical geometry (r, φ, z) in [10]:

$$\frac{\partial p(\rho)}{\partial r} - \frac{\rho u_\varphi^2}{r} = -\frac{\rho r}{(r^2 + z^2)^{3/2}}, \tag{4a}$$

$$\frac{\partial p(\rho)}{\partial z} = -\frac{\rho z}{(r^2 + z^2)^{3/2}}, \tag{4b}$$

where it is assumed that $\rho = \rho(r, z)$, $u_\varphi = u_\varphi(r)$, and $u_r = u_z = 0$.

Let $p(\rho) = k\rho^\gamma$ with $k > 0$, $\gamma \geq 1$, and

$$\zeta \in C^1(\bar{\Omega}_r),$$
$$\zeta(r) > 0, \quad r + \zeta(r)\zeta'(r) > 0 \quad \text{on} \quad \bar{\Omega}_r,$$

where $\Omega_r := (r_1, r_2)$, $r_1 > 0$.

1. For Eqs. (4) in the region $\{(r,z); r \in \bar{\Omega}_r, |z| \le \zeta(r)\}$, the solution

$$\rho(r,z) = \left[\frac{1}{k\gamma'}\left(\frac{1}{\sqrt{r^2+z^2}} - \frac{1}{\sqrt{r^2+\zeta^2(r)}}\right)\right]^{1/(\gamma-1)}, \quad (5)$$

$$u_\varphi(r) = \left[r\frac{r+\zeta(r)\zeta'(r)}{(r^2+\zeta^2(r))^{3/2}}\right]^{1/2}, \quad (6)$$

was found for $\gamma > 1$, where $\gamma' = \gamma/(\gamma-1)$. This solution has the property

$$\rho(r, \pm\zeta(r)) = 0 \quad \text{on} \quad \bar{\Omega}_r. \quad (7)$$

These formulas can easily be verified by rewriting Eqs. (4) in the form

$$k\gamma'\frac{\partial}{\partial r}\left(\rho^{\gamma-1}\right) - \frac{u_\varphi^2}{r} = -\frac{r}{(r^2+z^2)^{3/2}}, \quad (8)$$

$$k\gamma'\frac{\partial}{\partial z}\left(\rho^{\gamma-1}\right) = -\frac{z}{(r^2+z^2)^{3/2}}$$

in terms of the enthalpy $k\gamma'\rho^{\gamma-1}$.

Approximate solutions obtained by integrating (5) over z were used in [10, 12].

It turns out that it is possible to carry out the average of the solution over z *exactly*, such that the new solutions $\bar{\rho}(r) > 0$, $u_\varphi(r)$ obey the stationary equation

$$\frac{dp(\rho)}{dr} - \frac{\rho u_\varphi^2}{r} = \rho F(r) \quad \text{on} \quad \bar{\Omega}_r. \quad (9)$$

For this, we integrate Eq. (8) over the segment $[-\zeta(r), \zeta(r)]$ with fixed r and divide the result by $2\zeta(r)$. Using the property (7), we obtain

$$k\gamma'\frac{1}{2\zeta(r)}\frac{d}{dr}\int\limits_{-\zeta(r)}^{\zeta(r)}\rho^{\gamma-1}dz \quad (10)$$

$$-\frac{u_\varphi^2}{r} = -\frac{1}{r\sqrt{r^2+\zeta^2(r)}}.$$

We introduce the function

$$\bar{\rho}(r) := \left(\frac{1}{2\zeta(r)}\int\limits_{-\zeta(r)}^{\zeta(r)}\rho^{\gamma-1}(r,z)dz\right)^{1/(\gamma-1)}$$

$$= \left(\frac{1}{\zeta(r)}\int\limits_{0}^{\zeta(r)}\rho^{\gamma-1}(r,z)dz\right)^{1/(\gamma-1)}.$$

Raising both sides of (5) to the power $\gamma-1$ and integrating the result over z yields

$$\bar{\rho}(r) = \left(\frac{\lambda(r)}{k\gamma'}\right)^{1/(\gamma-1)}, \quad (11)$$

with

$$\lambda(r) := \frac{1}{\zeta(r)}\ln\left(\frac{\zeta(r)}{r} + \sqrt{\frac{\zeta^2(r)}{r^2}+1}\right) - \frac{1}{\sqrt{r^2+\zeta^2(r)}}. \quad (12)$$

We now rewrite the equality (10) in the form

$$k\gamma'\frac{d}{dr}\left(\bar{\rho}^{\gamma-1}\right) - k\gamma'\left(\frac{d}{dr}\frac{1}{\zeta(r)}\right)\zeta(r)\bar{\rho}^{\gamma-1}$$

$$-\frac{u_\varphi^2}{r} = -\frac{1}{r\sqrt{r^2+\zeta^2(r)}},$$

whence

$$k\gamma'\frac{d}{dr}\left(\bar{\rho}^{\gamma-1}\right) - \frac{u_\varphi^2}{r} = F(r)$$

$$:= -\frac{1}{r\sqrt{r^2+\zeta^2(r)}} - \frac{\zeta'(r)}{\zeta(r)}\lambda(r).$$

Thus the found the functions $\bar{\rho}$ and u_φ, see formulas (11), (12), and (6), also satisfy the stationary equation (9) with the introduced F.

2. When $\gamma = 1$ we fix $\rho_0 > 0$ and rewrite (4) in the form

$$k\frac{\partial}{\partial r}\ln\frac{\rho}{\rho_0} - \frac{u_\varphi^2(r)}{r} = -\frac{r}{(r^2+z^2)^{3/2}}, \quad (13)$$

$$k\frac{\partial}{\partial z}\ln\frac{\rho}{\rho_0} = -\frac{z}{(r^2+z^2)^{3/2}}.$$

By virtue of the first of these equations, we have

$$\ln\frac{\rho}{\rho_0} = \frac{1}{k}\left(\int\frac{u_\varphi^2(r)}{r}dr + \frac{1}{\sqrt{r^2+z^2}} + \psi(z)\right), \quad (14)$$

and by virtue of the second, we can take $\psi(z) = 0$ (a corresponding formula is given in [10]). Note that, according to (14), the function $\rho(r,z)$ then decreases with growth in $|z|$.

We will find a solution having the property

$$\rho(r, \pm\zeta(r)) = \rho_0 \quad \text{on} \quad \bar{\Omega}_r; \quad (15)$$

compare with (7). Substituting $z = \zeta(r)$ in (14) and differentiating both sides of the resulting equality with

respect to r, taking into account the above property, yields

$$\frac{u_\varphi^2(r)}{r} = -\frac{d}{dr}\frac{1}{\sqrt{r^2+\zeta^2(r)}}.$$

Therefore, as before, u_φ is specified by (6) (a minus sign can be written in its right-hand side if desired). The following formula now follows from (14) and (15):

$$\frac{\rho(r,z)}{\rho_0} = \exp\left[\frac{1}{k}\left(\frac{1}{\sqrt{r^2+z^2}} - \frac{1}{\sqrt{r^2+\zeta^2(r)}}\right)\right]; \quad (16)$$

compare with (5). With the same aim as in Part 1 above, we average the found solution over z. We introduce a function $\bar\rho$ such that

$$\frac{\bar\rho(r)}{\rho_0} := \exp\left(\frac{1}{2\zeta(r)}\int\limits_{-\zeta(r)}^{\zeta(r)} \ln\frac{\rho(r,z)}{\rho_0}dz\right) = \exp\left(\frac{1}{\zeta(r)}\int\limits_{0}^{\zeta(r)} \ln\frac{\rho(r,z)}{\rho_0}dz\right).$$

By virtue of (16), similar to (11), we obtain

$$\bar\rho(r) = \rho_0\exp\left(\frac{\lambda(r)}{k}\right). \quad (17)$$

Integrating (13) over the segment $z \in [-\zeta(r),\zeta(r)]$ with fixed r and dividing the result by $2\zeta(r)$ yields

$$k\frac{1}{2\zeta(r)}\int\limits_{-\zeta(r)}^{\zeta(r)}\frac{\partial}{\partial r}\ln\frac{\rho(r,z)}{\rho_0}dz - \frac{u_\varphi^2}{r} = -\frac{1}{2\zeta(r)}\int\limits_{-\zeta(r)}^{\zeta(r)}\frac{r}{(r^2+z^2)^{3/2}}dz.$$

Using the same reasoning as in Part 1, taking into account the property (15), we obtain

$$k\frac{d}{dr}\ln\frac{\bar\rho}{\rho_0} - \frac{u_\varphi^2}{r} = F \quad \text{on} \quad \bar\Omega_r$$

with the previous function F. Thus the found functions $\bar\rho$ and u_φ, see (17), (12), and (6), also satisfy the stationary equation (9) with $\gamma = 1$ and with this F.

3. REGULARIZED GAS-DYNAMICAL EQUATIONS AND METHOD FOR NUMERICAL SOLVING A PROBLEM

To numerically solve the Euler equations (1)–(3), we first construct the regularized (QGD) equations in a special way. These have the form

$$\frac{\partial\rho}{\partial t} + \nabla\cdot\mathbf{j}_m = 0, \quad (18)$$

$$\frac{\partial(\rho u_r)}{\partial t} + \nabla\cdot(u_r\mathbf{j}_m) + \frac{\partial p(\rho)}{\partial r} - \frac{\rho_* u_\varphi^2}{r} = \rho_* f_r + \nabla\cdot(\rho w_r^*\mathbf{u}) + \frac{\partial}{\partial r}\left(\tau c_s^2\nabla\cdot(\rho\mathbf{u})\right) - 2\rho\frac{u_\varphi}{r}w_\varphi^*, \quad (19)$$

$$\frac{\partial(\rho u_\varphi)}{\partial t} + \frac{1}{r}\nabla\cdot(ru_\varphi\mathbf{j}_m) + \frac{1}{r}\frac{\partial p(\rho)}{\partial\varphi} = \rho_* f_\varphi + \frac{1}{r}\nabla\cdot(r\rho w_\varphi^*\mathbf{u}) + \frac{1}{r}\frac{\partial}{\partial\varphi}\left(\tau c_s^2\nabla\cdot(\rho\mathbf{u})\right). \quad (20)$$

Here the regularized mass flux $\mathbf{j}_m$, density ρ_*, and regularized velocities are defined by the relations

$$\mathbf{j}_m = (j_{mr}, j_{m\varphi}), \quad j_{mr} = \rho(u_r - w_r),$$
$$j_{m\varphi} = \rho(u_\varphi - w_\varphi), \quad \rho_* = \rho - \tau\nabla\cdot(\rho\mathbf{u}),$$
$$w_r = \frac{\tau}{\rho}\left[\nabla\cdot(\rho u_r\mathbf{u}) + \frac{\partial p(\rho)}{\partial r} - \frac{\rho u_\varphi^2}{r} - \rho f_r\right],$$
$$w_\varphi = \frac{\tau}{\rho}\left[\frac{1}{r}\nabla\cdot(r\rho u_\varphi\mathbf{u}) + \frac{1}{r}\frac{\partial p(\rho)}{\partial\varphi} - \rho f_\varphi\right],$$
$$w_r^* = \tau\left[u_r\frac{\partial u_r}{\partial r} + \frac{1}{r}u_\varphi\frac{\partial u_r}{\partial\varphi} + \frac{1}{\rho}\frac{\partial p(\rho)}{\partial r} - \frac{u_\varphi^2}{r} - f_r\right],$$
$$w_\varphi^* = \tau\left[\frac{u_r}{r}\frac{\partial(ru_\varphi)}{\partial r} + \frac{u_\varphi}{r}\frac{\partial u_\varphi}{\partial\varphi} + \frac{1}{r\rho}\frac{\partial p(\rho)}{\partial\varphi} - f_\varphi\right].$$

The QGD system is closely related to the system of Euler equations, and differs from the latter in the inclusion of dissipative regularizing terms with a small coefficient—the parameter $\tau = \tau(r,\rho,\mathbf{u}) > 0$, which has the dimension of time. The exact solutions of the stationary Euler system are simultaneously the exact solutions of the stationary QGD system, according to the structure of its τ-dissipation. The conservation of momentum is satisfied for the QGD equations [16].

Note that a barotropic QGD system in Cartesian coordinates was proposed and studied in [19], and then investigated further in [20] and other studies.

The axially symmetric stationary solutions found in the previous section, $\rho = \rho(r)$, $u_r = 0$, $u_\varphi = u_\varphi(r)$ with $f_r = f_r(r)$ and $f_\varphi = 0$, are exact solutions not only of the Euler system, but also of its QGD expansion. Indeed, for such solutions, $w_\varphi = w_\varphi^* = 0$, and Eq. (19) reduces to Eq. (9) with $F = f_r$. Further, $w_r = w_r^* = j_{mr} = 0$, and therefore (18) and (20) are also satisified.

The initial boundary problem is set for the system (18)–(20) in the ring $\Omega_r \times [0, 2\pi)$. The condition of 2π periodicity of the solution in φ is specified.

The QGD approach makes it possible to apply a classical version of the finite-volume method approximating all flux terms using the central differences in space together with an explicit approximation in time. The sought gas-dynamical quantities refer to the computational nodes of a grid, and the fluxes are computed at the boundaries of cells at half-integer nodes. The τ terms ensure conditional stability of the constructed difference scheme. The scheme is written in a compact operator form in [18].

The regularization parameter is specified in the form

$$\tau = \tau(r, \rho, \mathbf{u}) = \alpha\sqrt{\Delta S}/\big(c_s + \sqrt{u_r^2 + u_\varphi^2}\big), \quad (21)$$
$$\Delta S = r\Delta r\Delta\varphi,$$

where the parameter $0 < \alpha < 0.5$ is chosen to facilitate stability and accuracy of the computations and ΔS is an estimate for the area of a grid cell in space ($\Delta r, \Delta\varphi$ are its steps).

4. RESULTS OF NUMERICAL SIMULATIONS

4.1. General Comments

In accordance with [11, 12], the problem was solved in the dimensionless variables $r = Rr'$, $t = t_0 t'$, $\rho = \rho_0\rho'$, $u_r = u_0 u_r'$, $u_\varphi = u_0 u_\varphi'$, and $p = p_0 p'$, where R is a characteristic spatial scale and the remaining factors are expressed by the formulas

$$t_0^2 = \frac{R^3}{GM}, \quad \rho_0 = \frac{M_0}{R^3}, \quad u_0^2 = \frac{GM}{R}, \quad p_0 = \frac{GM^2}{R^4},$$

where M_0 is a characteristic mass and G is the gravitational constant. The ranges of these quantities characteristic for astrophysics are $G = 6.67 \times 10^{-8}$ cm^3 g^{-1} s^{-2}, $M_0 = 2 \times 10^{33}$–6×10^{33} g, $R = 10^{11}$–10^{14} cm. The transition to the dimensionless variables does not change the form of the QGD system.

The computational domain is a ring $(r_1, r_2) \times [0, 2\pi)$ with $r_1 = 0.2$ and $r_2 = 1.4$.

In accordance with [11], the form of the initial gaseous cloud is specified by the function $\zeta(r) = \pm ar\exp(-b(r - r_0)^2)$, with $a = 0.2$, $b = 9.0$, and $r_0 = 0.8$; see Fig. 1. The forms of the corresponding stationary distributions of the density ρ and angular velocity u_φ are also presented in Fig. 1.

The initial distribution of ρ was taken in accordance with (11) ($\gamma > 1$), (17) ($\gamma = 1$), and (12). The initial distributions of the velocity components are $u_r^0 = 0$ and

$$u_\varphi^0(r, \varphi) = u_\varphi(r)\big(1 + Ae^{-b(r-r_0)^2}\sin(N_0\varphi)\big), \quad (22)$$

which is a perturbation of the stationary function u_φ; see (6). Compared to [11], the velocity perturbation has been smoothed over r. The parameter $A > 0$ is the amplitude and N_0 is the number of periods of the perturbation in $[0, 2\pi]$. The body force is specified in the form $f_r = F$ [see (9) and Fig. 1] and $f_\varphi = 0$.

"Soft" boundary conditions for the sought functions are specified at the ring boundaries. At the outer boundary, this provides virtually free passage of the perturbations through this boundary. The condition of 2π periodicity is specified over the azimuthal angle.

The grid was uniform in (r, φ), with $(N_r + 2) \times (N_\varphi + 1) = 80 \times 260$ nodes in the basic versions of the computations, and uniform in time t with a step of $\Delta t = 0.0005$; this value was not optimized. Fictitious nodes were used to specify the boundary conditions. The dimensionless time for the computations was restricted to $T = 10$. All the computations were carried out on a personal computer.

Note that the numerical computation of the flow with an initially unperturbed, stationary distribution was stable, with the density distributions at times $t = 0$ and $t = 10$ essentially coinciding.

4.2. Numerical Simulations of the Development of Perturbations

Further, we present the results of computations of the flow for the parameters of [11, 12], namely, for the case $\gamma = 5/3$, $k = 0.012$. In formula (22), we took $A = 0.1$ and $N_0 = 1$, 2, 3, 5, 7, and 10. We will also briefly describe the results in the shallow water approximation for $\gamma = 1$.

According to [4], typical values of c_s in a gaseous disk are of order 10 km/s for a rotational angular velocity ω of order 200 km/s, which corresponds to a Mach number M ~ 20. With such values of M, centrifugal instability can arise, referring to a class of unstable shear flows that develop when the angular velocity of the rotation is higher at the central part of the disk than at its periphery. Estimates show that, with $k = 0.012$, $\mathrm{M}_1 \sim 23$ and $\omega_1 \sim 11.5$ at the center of the disk and $\mathrm{M}_2 \sim 8$ and $\omega_2 \sim 0.6$ near its edge. Note that, due to our formulation of the problem, all forms of instability that are known in two-dimensional flows are automatically present in our computations, and are difficult to distinguish.

Reducing the perturbation amplitude A to 0.01 or increasing it to 0.2 leads to a proportional change in the density maxima without changing the physical picture of the solution.

Figure 2 shows the development of perturbations for $N_0 = 1$, 2, 3, 5, and 7. In all cases, a small initial perturbation introduced in u_φ leads to the development of large-scale structure and the formation

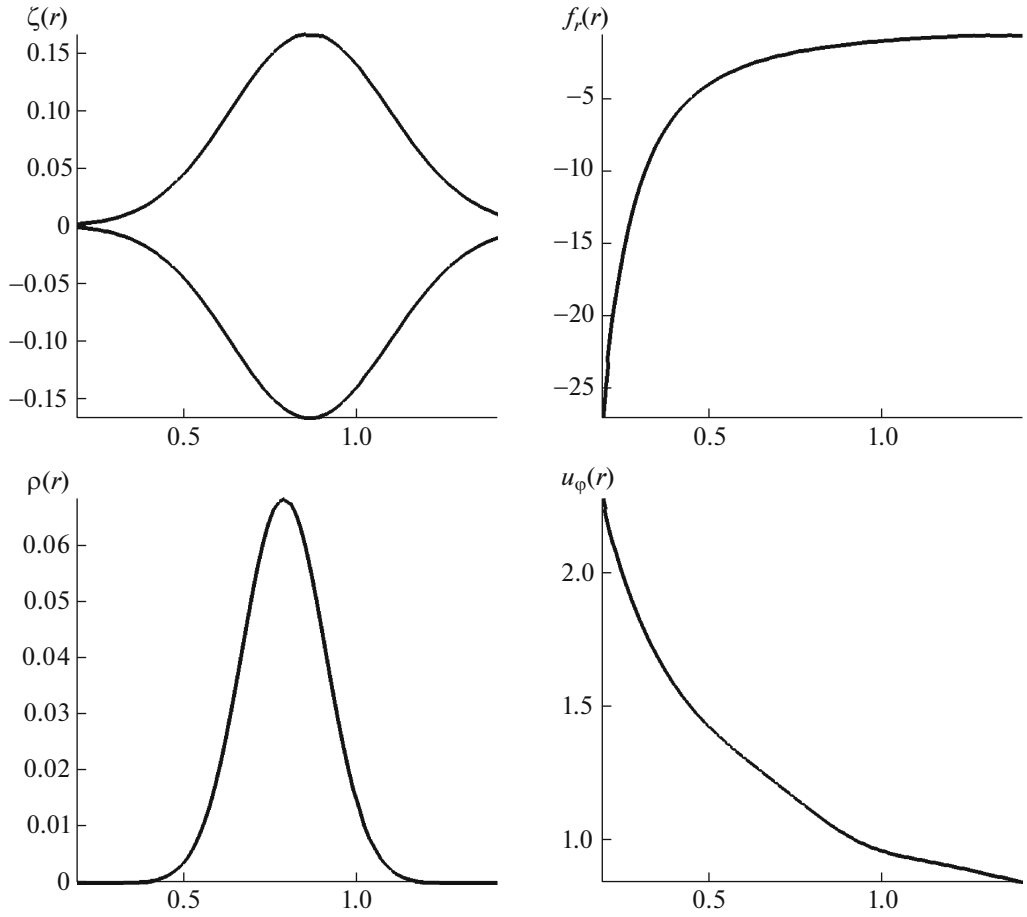

Fig. 1. Boundaries of the matter $\pm\zeta(r)$, the force $f_r(r)$, and the stationary distributions $\rho(r)$ and $u_\varphi(r)$ for $\gamma = 5/3$.

of lagging density arms with a characteristic aerodynamical shape. Bifurcation of the density maxima in the spiral arms can be seen; i.e., the formation of two density maxima in a single arm. This bifurcation develops from the beginning of an arm to its end. A similar effect is observed in real galaxies.

In the presented plots of the evolution of ρ, large-scale vortical structures form more freely with small N_0. Smaller structures form in the case of large N_0, which evolve into ring formations with time. For example, the evolution of ρ for $N_0 = 10$ is presented in Fig. 3 for $t = 0.6$, 1.1, 3, and 9.4. This shows the development of density perturbations and the formation of classical spiral arms in the form of lagging spirals. The system of arms becomes smoothed with time, and the distribution of ρ acquires the form of concentric rings at times $t \sim 8{-}9$.

The complex vortical structure of the solutions is clearly visible, although the spatial grid used is not very fine. This testifies to the fairly high accuracy of the algorithm in practice, in spite of the fact that it is formally only first order. It is important that the distribution of ρ at time $t = 1.1$ in Fig. 3 corresponds closely to the results of [13], where the solution was obtained using the full (not barotropic) Euler equations with a method of higher order accuracy on a similar spatial grid.

The last two plots in Fig. 3 present the distribution of u_r at time $t = 2.0$ and the typical distribution of u_φ, which varies little in time. We can see that u_r changes sign, which in principle can lead to the appearance of cyclonic vortices in the flow. The absence of such vortices in our computations is due to the fact that u_r is small in absolute magnitude, not exceeding 1% of u_φ (these perturbations are due to our formulation of the boundary conditions). Therefore, the stream lines in the flow obtained have shapes close to concentric circles.

The formation of large-scale structures in gaseous disks is accompanied by a redistribution of the instantaneous angular momentum, $M = r\rho u_\varphi$, and a shift of its maximum toward the inner boundary of the disk; this can facilitate the deposition of matter onto the central gravitational body. This transfer of M occurs due to the motion of the vortical structures without

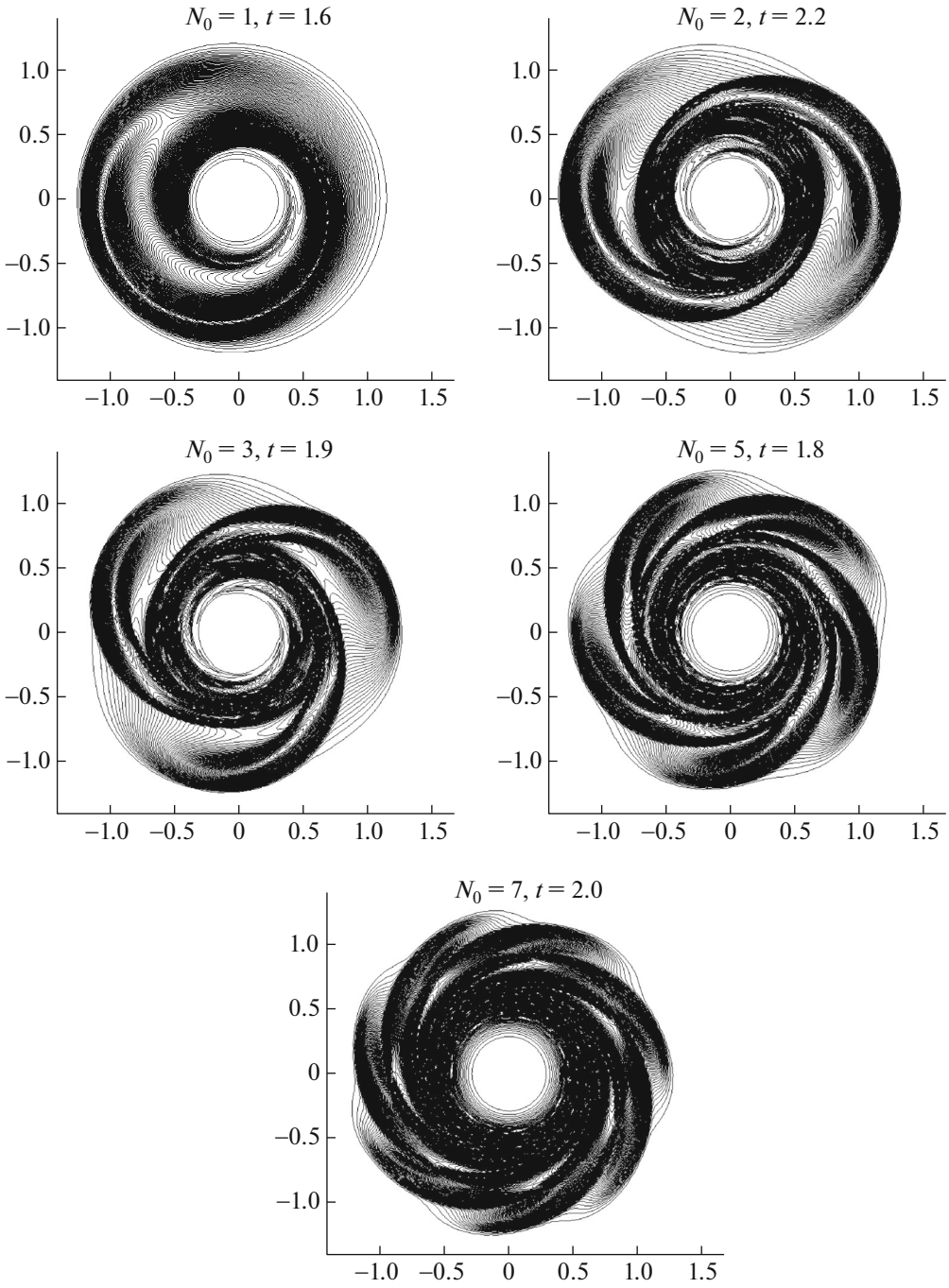

Fig. 2. Distributions of ρ for various N_0 and the indicated times t.

heating of the gas, which is small in our model. Figure 4 presents plots of M (for $\varphi = 0$) for three characteristic times and for all the considered values of N_0. The most intense transfer of M is observed for small N_0, when the largest vortical structures form together with pronounced arms in the density distribution. The transfer of M is hindered when $N_0 = 10$ due to the mutual influence of the vortices that are arising.

The main computations were carried out with $\alpha = 0.3$ in the formula for τ (21). Reducing α to 0.1 leads to the appearance of oscillations of the numerical solution. Increasing α to 0.4 smooths the numerical solution somewhat, and further increase in α leads to excessive smearing of ρ. Making the spatial grid more dense leaves the flow pattern essentially unchanged, confirming the adequacy of our choice of grid.

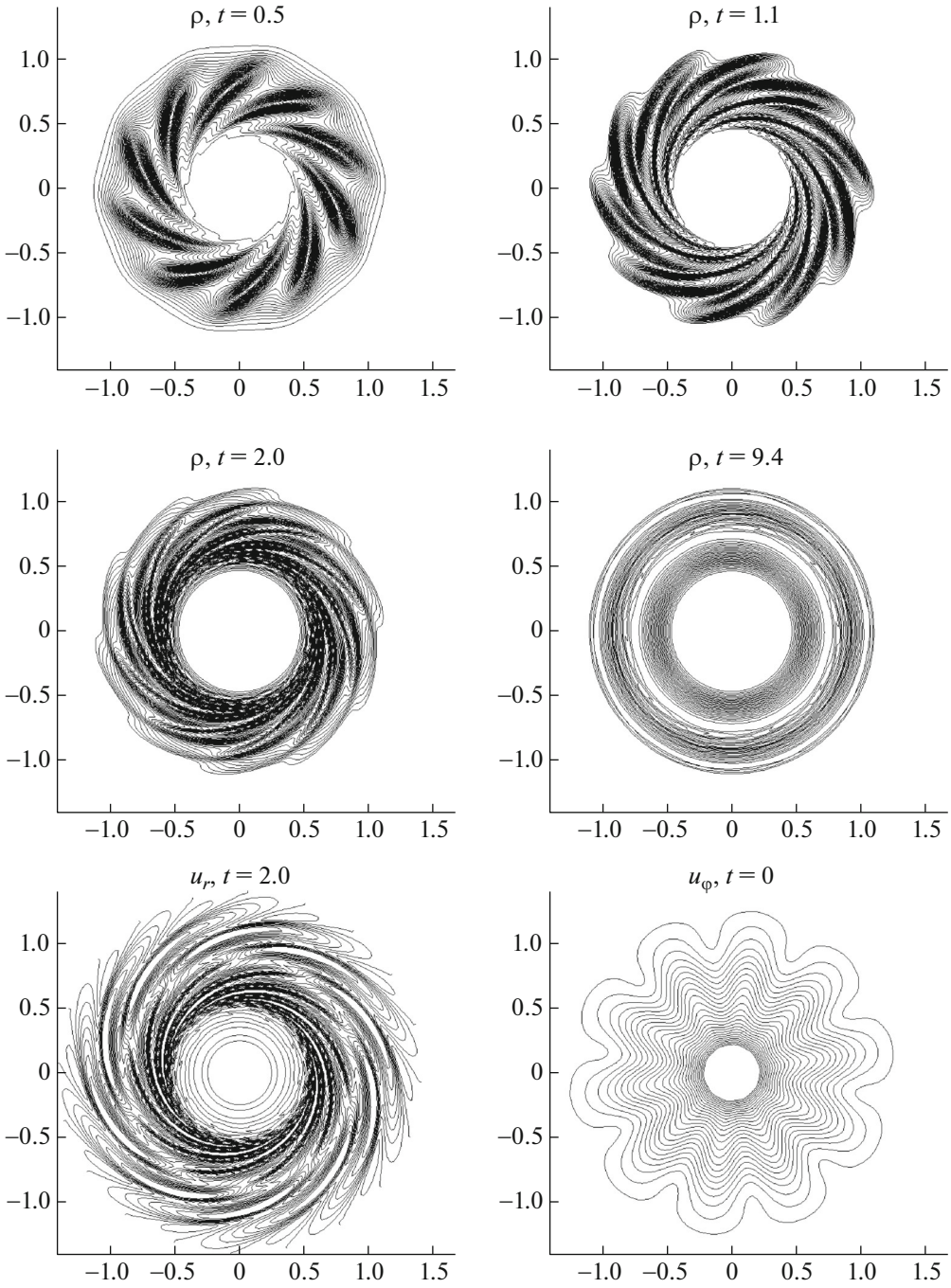

Fig. 3. Distributions of ρ for $t = 1.0$, 1.1, 2.0, and 9.4 and distributions of u_r for $t = 2.0$ and of u_φ for $t = 0.0$, for $N_0 = 10$.

4.3. Shallow-Water Approximation and Isothermal Case

Natural experiments with shallow water were used in [2, 4] to analyze vortical flows in accretion disks. Comparison of the results of the numerical simulations for the same problem solved using gas-dynamical equations and the equations for the shallow-water approximation can help us analyze the correctness of such an approach.

For the barotropic system of equations used, the value $\gamma = 5/3$ corresponds to the flow of an ideal gas, while $\gamma = 2$ can be used to model a hydrodynamical flow in the shallow-water approximation, when the density of the gas ρ depends on the thickness of a layer of fluid h in meters and the pressure is given by the hydrostatic formula $p = gh^2/2$, that is, $k = g/2$, where $g = 9.8$ m/s^2 is the acceleration due to gravity.

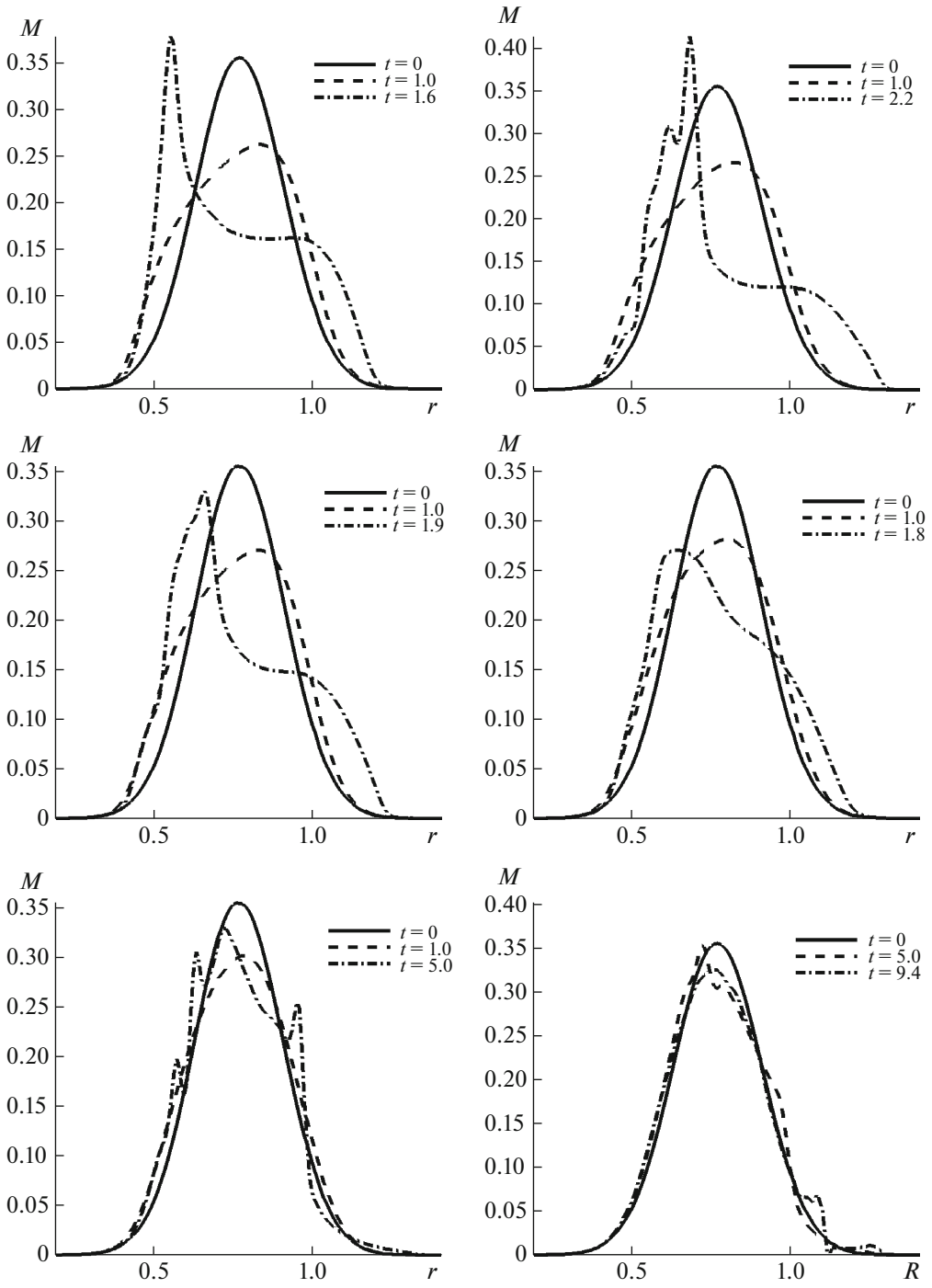

Fig. 4. Distributions of the angular momentum for $N_0 = 1$, 2, 3, 5, 7, and 10, respectively.

We computed an annular channel with radii $r_1 = 0.2$ m and $r_2 = 1.4$ m. The resulting flow pattern turned out to be close to that for the case $\gamma = 5/3$ in Fig. 3, including when $N_0 = 10$. This and other computations confirm the possibility of applying the shallow-water approximation to analyze gas-dynamical processes in galactic clouds.

In the case of an isothermal flow ($\gamma = 1$), the form of the original equations is simplified, and the sound speed becomes constant: $c_s = \sqrt{k}$. The stationary density distribution (17) contains two free parameters: ρ_0 and k. Variations in ρ_0 lead to proportional changes in the total mass of the gaseous disk, and increasing k makes the form of the density distribution

in the disk more uniform in the radial direction and decreases the total mass of gas.

A series of numerical computations was carried out for $\gamma = 1$ with $N_0 = 10$ for ρ_0 values in the range $0.01-1$ and $k = 0.012$ and 0.12. The results show that the bifurcation of the arms is manifest more strongly in disks with lower masses with more uniform radial density distributions in the disk.

More detailed information on the numerical results is given in [18].

5. CONCLUSION

We have studied hydrodynamical aspects of the formation of spiral–vortical structures using numerical simulations of the formation of structures in an accretion disk based on a relatively simple model—two-dimensional barotropic Euler equations with a body force.

We have derived new axially symmetric stationary solutions of these equations in the isentropic and isothermal cases.

These solutions were used as initial distributions in the non-stationary problem, introducing small perturbations in the azimuthal velocity distribution. Our numerical simulations have demonstrated the development of these perturbations and the resulting formation of large-scale structures in the form of lagging spirals—density arms having a characteristic aerodynamical form. The bifurcation of the density arms was observed, as well as the transfer of momentum from the central region of the disk to its inner boundary. This latter effect is due to the development of large-scale vortical structures in the flow, and occurs more intensively in the case of weakly oscillating azimuthal perturbations.

We have also verified that the shallow-water approximation gives a flow pattern close to the gas-dynamical results. This confirms the possibility of using shallow-water experiments to model gas-dynamical processes in galactic clouds.

The numerical algorithm used is based on the application of regularized Euler equations, in other words, quasi-gas-dynamical equations. It is completely general, and enables numerical simulations of a variety of flows of interest in astrophysics, with various initial distributions and attractive forces, on a personal computer.

ACKNOWLEDGMENTS

We thank V.M. Chechetkin and A.Yu. Lugovskii for attracting our attention to this subject, and also for discussions of the formulation of the problem and the results obtained. This work was supported by the Russian Foundation for Basic Research (grant 16-01-00048).

REFERENCES

1. N. I. Shakura and R. A. Syunyaev, Astron. Astrophys. **24**, 337 (1973).
2. A. M. Nezlin and E. N. Snezhkin, *Vortexes and Spiral Structures. Astrophysics and Plasma Physics in Shallow Water Experiments* (Nauka, Moscow, 1990; Springer, Berlin, Heidelberg, 1993).
3. O. M. Belotserkovskii, A. M. Oparin, and V. M. Chechetkin, *Turbulence. New Approaches* (Nauka, Moscow, 2003; Cambridge International Science, Cambridge, 2005).
4. A. M. Fridman, Phys. Usp. **50**, 115 (2007).
5. A. M. Fridman and D. V. Bisikalo, Phys. Usp. **51**, 551 (2008).
6. D. V. Bisikalo, A. G. Zhilkin, and A. A. Boyarchuk, *Gas Dynamics of Close Binary Stars* (Fizmatlit, Moscow, 2013) [in Russian].
7. D. N. Razdoburdin and V. V. Zhuravlev, Phys. Usp. **58**, 1031 (2015).
8. A. V. Kolesnichenko, *Some Problems in the Structure of Continuous Cosmic Media. Simulations of Protoplanetary Accretion Disks* (Inst. Prikl. Mat. im. M.V. Keldysha, Moscow, 2017) [in Russian].
9. V. V. Zhuravlev and N. I. Shakura, Astron. Lett. **33**, 673 (2007).
10. M. V. Abakumov, S. I. Mukhin, Yu. P. Popov, and V. M. Chechetkin, KIAM Preprint No. 33 (Keldysh Inst. Appl. Math., Moscow, 1995) [in Russian].
11. M. V. Abakumov, S. I. Mukhin, Yu. P. Popov, and V. M. Chechetkin, Mat. Model. **10** (5), 35 (1998).
12. E. P. Velikhov, A. Yu. Lugovsky, S. I. Mukhin, Yu. P. Popov, and V. M. Chechetkin, Astron. Rep. **51**, 154 (2007).
13. A. Yu. Lugovsky and Yu. P. Popov, Comput. Math. Math. Phys. **55**, 1407 (2015).
14. B. N. Chetverushkin, *Kinetic Schemes and Quasi-Gas-Dynamical Systems of Equations* (MAKS Press, Moscow, 2004) [in Russian].
15. T. G. Elizarova, *Quasi-Gas Dynamic Equations* (Nauchnyi Mir, Moscow, 2007; Springer, Berlin, Heidelberg, 2009).
16. Yu. V. Sheretov, *Dynamics of Continuous Media with Spatial and Temporal Averaging* (Regulyarn. Khaotich. Dinamika, Moscow, Izhevsk, 2009) [in Russian].
17. T. G. Elizarova and O. V. Bulatov, Comput. Fluids **46**, 206 (2011).
18. T. G. Elizarova, A. A. Zlotnik, and M. A. Istomina, KIAM Preprint No. 1 (Keldysh Inst. Appl. Math., Moscow, 2017) [in Russian].
19. A. A. Zlotnik and B. N. Chetverushkin, Comput. Math. Math. Phys. **48**, 420 (2008).
20. A. A. Zlotnik, Mat. Model. **24** (4), 65 (2012) [in Russian].

Translated by D. Gabuzda